

PAPER • OPEN ACCESS

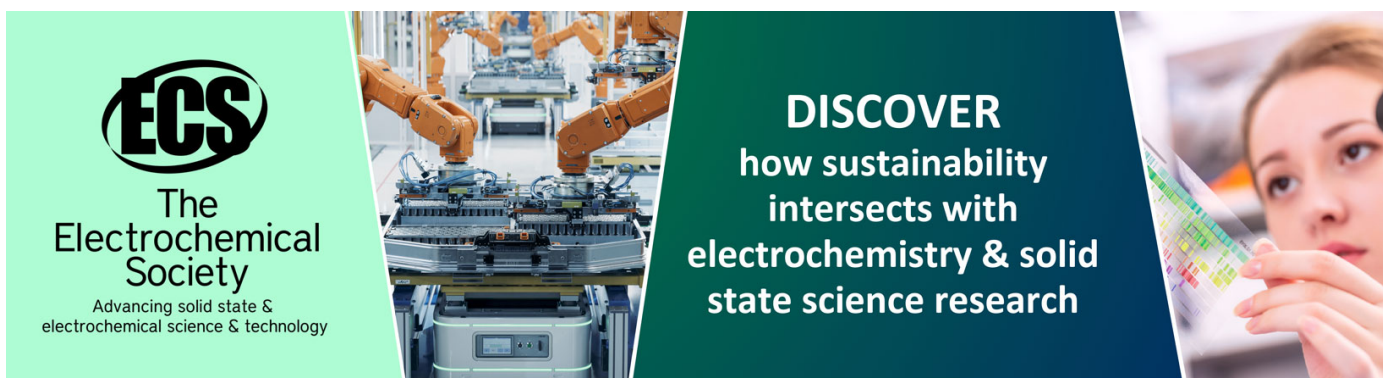
## Monolithic HV-CMOS sensors for a beam monitoring system of therapeutic ion beams

To cite this article: B. Topko *et al* 2024 *JINST* **19** C03043

View the [article online](#) for updates and enhancements.

You may also like

- [Development of a novel fibre optic beam profile and dose monitor for very high energy electron radiotherapy at ultrahigh dose rates](#)  
Joseph J Bateman, Emma Buchanan, Roberto Corsini et al.
- [Measurement of UKRI-MPW0 after irradiation: an HV-CMOS prototype for high radiation tolerance](#)  
C. Zhang, J. Hammerich, S. Powell et al.
- [Intelligent low-level RF system by non-destructive beam monitoring device for cyclotrons](#)  
M. S. Sharifi Asadi Malafeh, M. Ghergherehchi, H. Afarideh et al.






**ECS**  
The  
Electrochemical  
Society  
Advancing solid state &  
electrochemical science & technology

**DISCOVER**  
how sustainability  
intersects with  
electrochemistry & solid  
state science research

24<sup>TH</sup> INTERNATIONAL WORKSHOP ON RADIATION IMAGING DETECTORS  
OSLO, NORWAY  
25–29 JUNE 2023

## Monolithic HV-CMOS sensors for a beam monitoring system of therapeutic ion beams

B. Topko <sup>a,\*</sup> M. Balzer,<sup>b</sup> A. Dierlamm <sup>a,b</sup> F. Ehrler,<sup>b</sup> U. Husemann <sup>a</sup> R. Koppenhöfer,<sup>a</sup> I. Perić,<sup>b</sup> M. Pittermann<sup>a</sup> and J. Naumann<sup>c</sup>

<sup>a</sup>*Institute of Experimental Particle Physics (ETP), Karlsruhe Institute of Technology (KIT),  
76131 Karlsruhe, Germany*

<sup>b</sup>*Institute for Data Processing and Electronics (IPE), Karlsruhe Institute of Technology (KIT),  
76131 Karlsruhe, Germany*

<sup>c</sup>*Heidelberg Ion-Beam Therapy Center (HIT),  
Department of Radiation Oncology, Heidelberg University Hospital,  
69120 Heidelberg, Germany*

E-mail: [bogdan.topko@kit.edu](mailto:bogdan.topko@kit.edu)

**ABSTRACT.** Nowadays, cancer treatment with ion beam is well established and studied. This method allows to deposit the maximum dose to the tumor and minimize the damage to healthy tissue, due to the Bragg peak of the ion energy deposition near the end of the particle range. During the treatment, it is possible to provide volumetric dose delivery by changing the particle energy (penetration depth) and adjusting the beam position via a magnetic system. For the beam monitoring system, the precise measurement of the beam direction, shape and fluence in real time becomes crucial to provide effective and safe dose delivery to the tumor. Additionally, the system should work for beam intensities up to  $10^{10} \text{ s}^{-1}$  for protons, be tolerant to 1 MeV neutron equivalent fluences up to  $10^{15} \text{ cm}^{-2}$  per year and be tolerant to magnetic fields (for MR-guided ion beam).

The studies presented in this article are focused on the application of the HitPix sensor family with counting electronics and frame-based readout for such a beam monitoring system. The HitPix sensors are monolithic pixelated silicon sensors based on HV-CMOS technology and have been developed at the ASIC and Detector Lab (ADL, KIT). Recent measurements with ion beams and a multi-sensor readout as well as future developments are discussed.

**KEYWORDS:** Instrumentation for hadron therapy; Pixelated detectors and associated VLSI electronics; Solid state detectors

\*Corresponding author.

---

## Contents

<b>1</b>	<b>Introduction</b>	<b>1</b>
<b>2</b>	<b>Microbeam test</b>	<b>1</b>
<b>3</b>	<b>Radiation hardness</b>	<b>3</b>
<b>4</b>	<b>Multi-sensor readout</b>	<b>5</b>
<b>5</b>	<b>Conclusion</b>	<b>7</b>

---

## 1 Introduction

Modern ion beam therapy enables maximum dose delivery to the cancer cells while minimizing damage of surrounding healthy tissue, due to the Bragg peak of the ion energy deposition near the end of the particle range [1]. The ongoing developments of MR-guided ion beam therapy promise significant improvements of the cancer treatment by combining the unparalleled soft-tissue contrast and real-time imaging capabilities of MRI with the most conformal dose distribution and best dose steering capability provided by modern ion beam therapy [2]. In order to ensure the treatment's accuracy and safety in such systems, the ion beam monitoring system should precisely and continuously measure the beam's real-time position, shape, and integrated dose.

Reference [3] summarizes the proposed beam monitor for the Heidelberg Ion-Beam Therapy Center (HIT) based on HV-CMOS sensors [4, 5], an overview of its advantages for traditional and MR-guided ion beam therapy, the description of the HitPix sensor family, which were developed at the ASIC and Detector Lab (ADL, KIT), and first evaluation results of HitPix2 performance.

The studies presented here continue the research started in [3] and focus on resolving the discovered HitPix2 sensor issues in order to prepare the next HitPix3 sensor design. They include proton microbeam tests of HitPix pixel structures and ion beam tests of irradiated HitPix2 sensors with different resistivities. The multi-sensor readout was tested with a  $2 \times 5$  matrix of HitPix2 sensors at HIT for a future beam monitor demonstrator. The beam monitor demonstrator with  $5 \times 5$  HitPix3 sensors for long-term operation in the quality assurance room at HIT will be the next development step towards a full-scale beam monitor [3].

## 2 Microbeam test

Measurements of HitPix2 sensors with ion beams at HIT revealed a significant loss in detection efficiency at high particle rates [3]. This loss is caused by a baseline drop of the first stage amplifier when the sensor is hit by an ion beam at high intensity. The in-air proton microbeam at Ruder Bošković Institute [6] was used in order to determine the region with a typical size of  $O(\mu\text{m}^2)$  and the corresponding signal processing structure which is responsible for the baseline drop of the in-pixel amplifier when hit by ions.

**Setup description.** The experimental setup mainly consists of a HitPix sensor carrier placed next to the microbeam nozzle, an FPGA board for control and readout, a mechanical stage, a power supplies, a control PC and an oscilloscope. It is shown in figure 1.

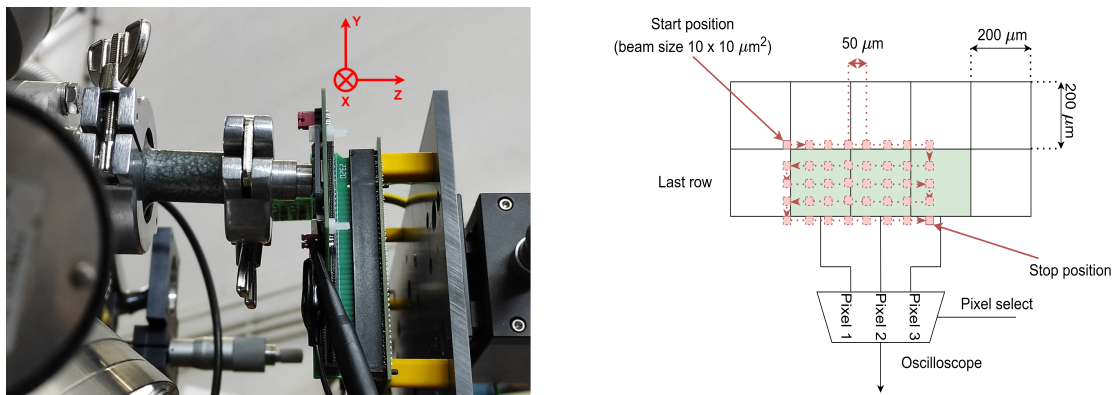


**Figure 1.** Microbeam nozzle and HitPix2 sensor carrier (left), pixels scanning procedure (right).

**Tested samples.** The HitPix1 and HitPix2 samples were tested at the microbeam setup. A pixel of each HitPix sensor consists of three main functional blocks: collection diode, analogue electronics (amplifier and comparator) and digital electronics (hit counter and adder) [7]. The HitPix1 sensors were designed in two flavors with standard (STD) and isolated (ISO) pixel topologies and pMOS based amplifier circuit [8]. The STD pixel contains each functional block in an individual n-well. The ISO pixel provides an additional deep p-well isolating the shallow n-wells from the common deep n-well [7]. The HitPix2 sensors were designed only with STD pixel topology and nMOS based amplifier circuit [8].

**Measurement procedure.** In the first step, the sensor position was manually adjusted along the beam ( $z$ ) axis to bring the sensor as close as possible to the beam nozzle in order to reduce the beam particle scattering and energy loss in air. After that, the sensor was moved to the scanning start position along the  $x$  and  $y$  axes with remote control of the mechanical stage by monitoring a single pixel's counts with a control software. The output voltage of the charge sensitive amplifier was measured for the pixels of the row closest to the sensor's periphery electronics. The scanning of single pixels with an area of  $200 \times 200 \mu\text{m}^2$  was performed in a grid by moving the sensor under test in  $50 \mu\text{m}$  steps, while irradiated with an ion beam with size of  $10 \times 10 \mu\text{m}^2$  and constant reproducible intensity. The modes of signals and baseline drops frequencies ( $f_{\text{drop}}$ ) over 10 waveforms were recorded by an oscilloscope for three neighboring pixels at each beam position. Figure 1 shows the schematic view of the measurement procedure. This measurement was repeated for each sample and beam energies (1–3 MeV protons). The 1 MeV proton beam will not be further discussed, since it hardly penetrated the passivation, metal- and transistor layers to reach the sensitive volume. The example of a pixel  $f_{\text{drop}}$  map as a function of the beam position (after linear interpolation) and the approximate locations of a main pixel functional blocks are shown in figure 2 on the left. Additionally a waveform of the in-pixel amplifier signals and baseline drops for HitPix2 are shown in figure 2 on the right. The region with high  $f_{\text{drop}}$  has rectangular shape and an approximately size of  $200 \times 100 \mu\text{m}^2$ , which partially covers the sensor diode and the transition area between the diode and the in-pixel electronics.

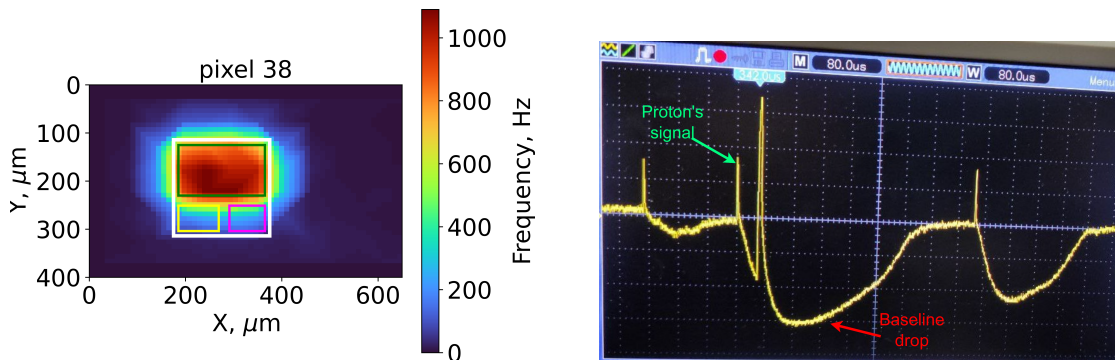


**Figure 2.** Linearly interpolated  $f_{\text{drop}}$  map for HitPix2 pixel with approximate locations of collection diode, analogue and digital electronics — green, magenta and yellow rectangles, respectively (left). Waveform of the in-pixel amplifier signals and baseline drops (right) corresponding to beam position  $X = 200 \mu\text{m}$ ,  $Y = 200 \mu\text{m}$ . Sensor  $V_{\text{bias}} = -50 \text{ V}$ . Proton microbeam parameters: intensity =  $1.4 \times 10^3 \text{ s}^{-1}$ ; energy = 3 MeV.

Table 1 shows results of the measurements in the discovered high  $f_{\text{drop}}$  region for each HitPix flavor. The measurements of HitPix1 confirmed the location of the baseline drops, but revealed also a higher tolerance to this negative effect of the HitPix1 sensor (especially with ISO pixel topology), since the maximum frequency of baseline drops was much smaller than for HitPix2.

**Table 1.**  $f_{\text{drop}}$  for different HitPix flavors in proton beam.

Sensor	Pixel	$E_{\text{beam}}$ , MeV	$I_{\text{beam}}$ , $\text{s}^{-1}$	Min. $f_{\text{drop}}$ , kHz	Max. $f_{\text{drop}}$ , kHz
HitPix2	STD	3	$1.4 \times 10^3$	$0.90 \pm 0.07$	$1.10 \pm 0.07$
HitPix1	STD	3	$1.4 \times 10^3$	$0.10 \pm 0.02$	$0.20 \pm 0.02$
HitPix1	ISO	3	$1.4 \times 10^3$	$0.0 \pm 0.0$	$0.0 \pm 0.0$

### 3 Radiation hardness

HitPix sensors with different resistivities were uniformly irradiated with 23 MeV protons at Zyklotron AG (ZAG)<sup>1</sup> in order to determine the most radiation tolerant substrate for the next sensor design. The 1 MeV neutron equivalent fluence was  $\sim 1 \times 10^{15} \text{ cm}^{-2}$ , equivalent to 1 year of operation in the beam center of HIT. The previous measurements [3] with irradiated samples showed an increase in leakage current at room temperature by a factor of 1000, which led to limited operation voltage (below 25 V), high threshold values need for in-pixel comparator to omit noise and, as a consequence, reduced detection efficiency for irradiated sensors. A final conclusion about the most suitable substrate resistivity could not be found at room temperature [3]. In the following measurements, sensors were cooled and tested at HIT beam test with carbon ions at different energies. A cooling box contained a reference HitPix sensor with a temperature sensor mounted to its surface. Before each measurement with the beam the current-voltage  $I(V)$  characteristic of each tested sample at the beamline was measured. The final temperatures of the sensors under test  $T_{IV}$  were extracted from  $I(V)$  curves by using the formula of temperature dependence of the leakage current [9] and using the information from the reference temperature sensor  $T_{\text{ref}}$  for calibration of initial  $I(V)$  curves at room temperature. The  $I(V)$  curves (in absolute values) are shown in figure 3.

<sup>1</sup><https://www.zyklotron-ag.de/index.php>, accessed on 18 September 2023.

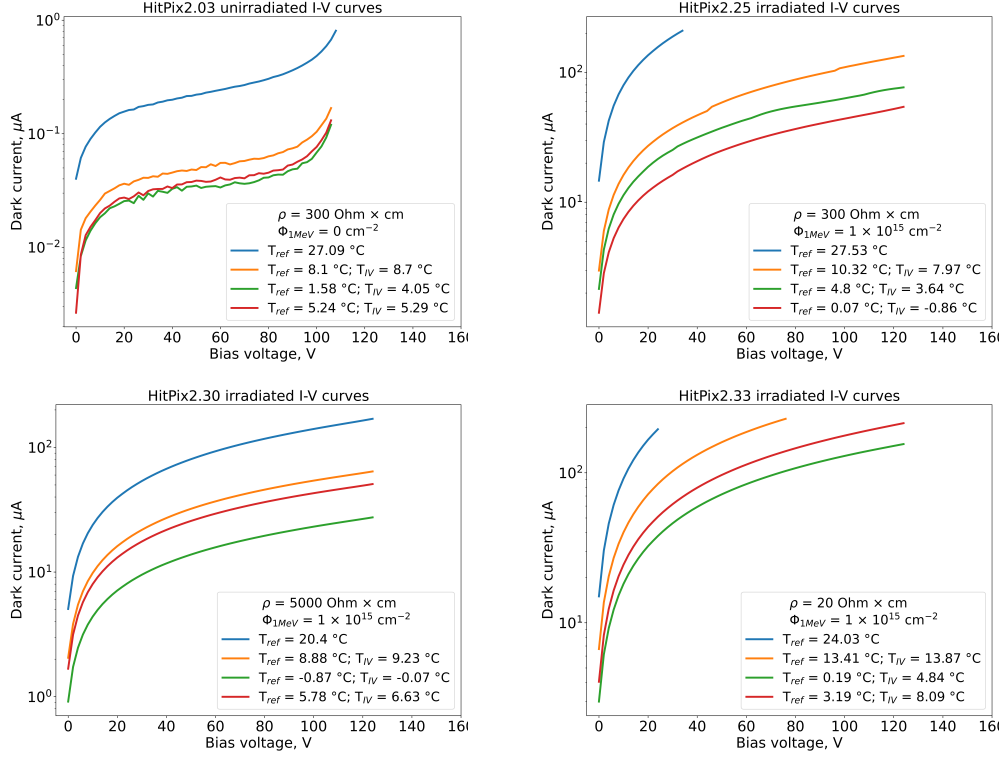


**Figure 3.** I(V) curves (in absolute values) of reference unirradiated sensor HitPix2.03 with resistivity of  $\rho = 300 \text{ Ohm} \times \text{cm}$  (top left) and irradiated sensors HitPix2.25 with  $\rho = 300 \text{ Ohm} \times \text{cm}$  (top right), HitPix2.30 with  $\rho = 5000 \text{ Ohm} \times \text{cm}$  (bottom left), HitPix2.33 with  $\rho = 20 \text{ Ohm} \times \text{cm}$  (bottom right) at different temperature.

After the I(V) measurements, each sensor recorded 1000 frames with a  $350 \mu\text{s}$  long counting period each and without a beam in order to identify noisy pixels, which were excluded from the following detection efficiency analysis. For each pixel at the given in-pixel comparator threshold (only one threshold value could be set for all HitPix2 pixels) the pixel hit rate ( $\text{pix\_hr}$ ) was averaged over the frames according to the equation (3.1).

$$\langle \text{pix\_hr} \rangle = \frac{1}{N_{\text{frames}}} \sum_{i=1}^{N_{\text{frames}}} \text{pix\_hr}_i \quad (3.1)$$

If a pixel had  $\langle \text{pix\_hr} \rangle > 0.05$  counts per frame it was marked as noisy. It is important to point out that these noisy pixels were still fully functional, but the common threshold was set too low for them, due to a process dependent variation of the amplifier gain of each pixel, which becomes significant if one needs to lower the threshold to detect smaller signals.

All sensors under test were exposed to steady carbon ion beam at different energies. The relative beam shape was controlled to stay within 0.8–0.9 cm full width at half maximum (FWHM). The detection efficiency was calculated for each irradiated sensor with equation (3.2), where 100% efficiency corresponds to the median of  $\langle \text{pix\_hr} \rangle$  of a non-irradiated sensor at room temperature.

$$\text{Efficiency} = 100\% \cdot \frac{\text{median}(\{\langle \text{pix\_hr} \rangle_{j,\text{irrad}} | j \notin \text{noisy}\})}{\text{median}(\{\langle \text{pix\_hr} \rangle_{k,\text{unirrad}} | k \notin \text{noisy}\})} \quad (3.2)$$

The calculated efficiencies of irradiated samples at the lowest temperature are shown in figure 4. The efficiency is decreasing with increasing beam energy, since the ionization signal is reduced at higher energy. The fraction of excluded noisy pixels for each sample is as follows: 27.0% for  $\rho = 300 \text{ Ohm} \times \text{cm}$ , 17.3% for  $\rho = 5000 \text{ Ohm} \times \text{cm}$  and 34.4% for  $\rho = 20 \text{ Ohm} \times \text{cm}$ . The sensor implemented on 300 Ohm  $\times$  cm substrate has the highest efficiency after irradiation (close to 80% at the lowest energy and about 60% at the highest energy). From these results some conclusions can be drawn: 1) for the new sensor design an individual pixel threshold tuning is required in order to reduce the fraction of masked noisy pixels; 2) sensors based on 300 Ohm  $\times$  cm substrate have the best performance after irradiation.

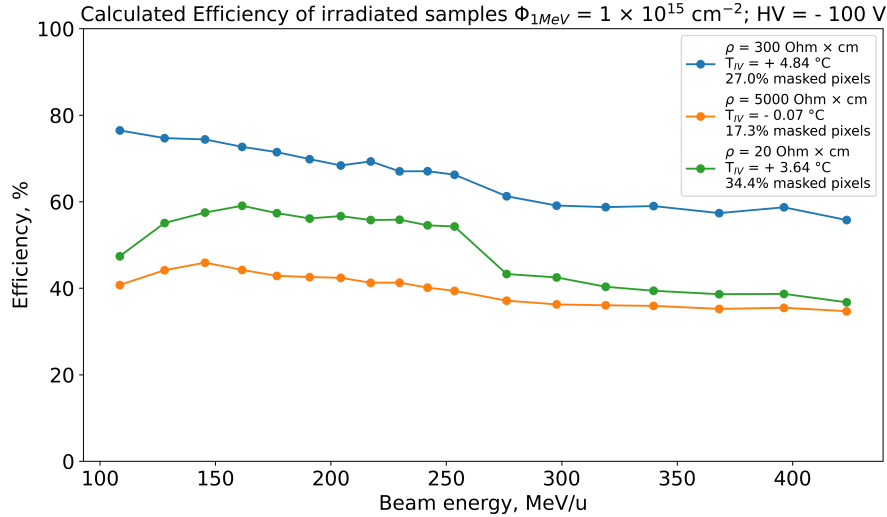


**Figure 4.** Calculated detection efficiency of cooled irradiated samples measured with carbon beam at different energies. Beam intensity =  $5.0 \times 10^6 \text{ s}^{-1}$ . The beam shape was adapted w.r.t. the beam energy to stay within 0.8–0.9 cm FWHM.

#### 4 Multi-sensor readout

The matrix prototype of HitPix2 sensors was assembled to test the multi-sensor readout and beam monitoring performance. It consists of two rows with five sensors each as shown in figure 5. Sensors in one row are connected in daisy chain mode — the input of the readout shift register (data\_in) of one sensor is directly connected to the output of the readout shift register (data\_out) of the previous sensor. All control signals, for example readout clocks, counter/adder selection etc., form a bus and are connected to all sensors in parallel. The row data is shifted through the whole chain during the readout procedure. This method simplifies a readout logic and reduces a number of readout traces. The readout row structure is shown in figure 5 in simplified form.

At HIT, the beam position and shape in  $x$ - and  $y$ -directions are monitored with two multi-wire proportional chambers (MWPCs) [10]. In order to estimate the  $2 \times 5$  matrix performance, all measurements (different focus settings and ion types) were performed with the  $2 \times 5$  matrix and a third, movable MWPC located at the focal point of the beam line. During the measurements, the frame size of the  $2 \times 5$  matrix was set to  $350 \mu\text{s}$ . The example of a measured proton beam profile with the  $2 \times 5$  matrix in one frame and 2D Gaussian fit are shown in figure 6. The red dashed lines

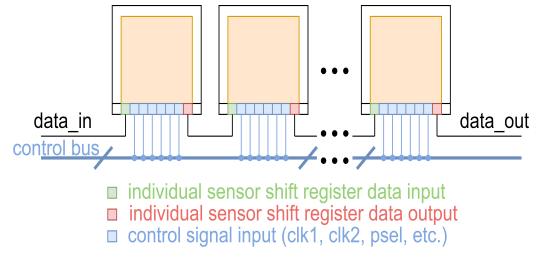
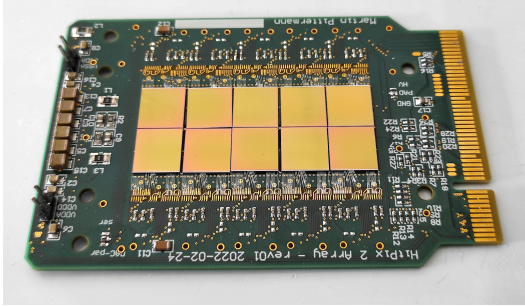


**Figure 5.** Assembled  $2 \times 5$  HitPix2 matrix (left). Simplified view of daisy chain readout principle (right).

in the plot correspond to active areas of the sensors. The sensor positions were measured with a microscope in order to take into account local shifts and rotations, since the sensors were assembled into the matrix manually. Noisy pixels were masked during analysis.

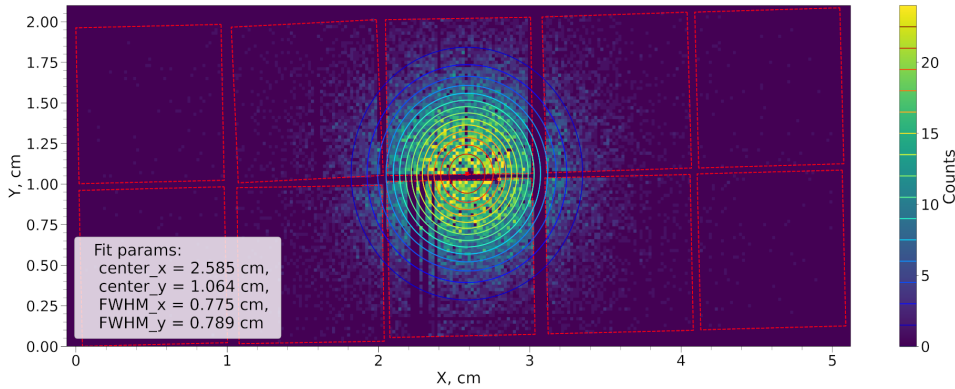


**Figure 6.** Proton beam profile measured with  $2 \times 5$  matrix in one  $350 \mu\text{s}$  frame and its 2D Gaussian fit. Matrix  $V_{\text{bias}} = -100 \text{ V}$ . Red dashed lines corresponds to active areas of the sensors. Nominal beam parameters: intensity =  $2.0 \times 10^8 \text{ s}^{-1}$ ; energy =  $221.06 \text{ MeV/u}$ ; FWHM =  $0.81 \text{ cm}$ .

Each non-empty frame (beam was delivered in spills) was fitted with a 2D Gaussian function with the coordinates of the beam center and FWHM in  $x$ - and  $y$ - direction as the fit parameters. The mean and the standard deviation  $\sigma$  of FWHM in  $x$ - and  $y$ - direction were calculated over all non-empty frames. A comparison of the determined mean and  $\pm 1.5 \sigma$  of FWHM in  $x$ - and  $y$ - directions of proton and carbon beams with the MWPC and the  $2 \times 5$  matrix at different beam focus settings is shown in figures 7 and 8, respectively. Both FWHM  $x$  and FWHM  $y$  measured with the MWPC and the  $2 \times 5$  matrix follow the same distributions. The deviation of FWHM  $y$  measured with the  $2 \times 5$  matrix increases at large nominal beam width, because the wide beam did not fit the matrix size in  $y$ - direction. The FWHM  $y$  deviation of the carbon beam at large nominal beam width measured with the  $2 \times 5$  matrix is larger than for the proton beam, since the intensity of the carbon beam was 40 times lower, which led to poor statistics within one frame. From these results it is concluded that the matrix based on HitPix2 matches the HIT requirements for the beam shape reconstruction.



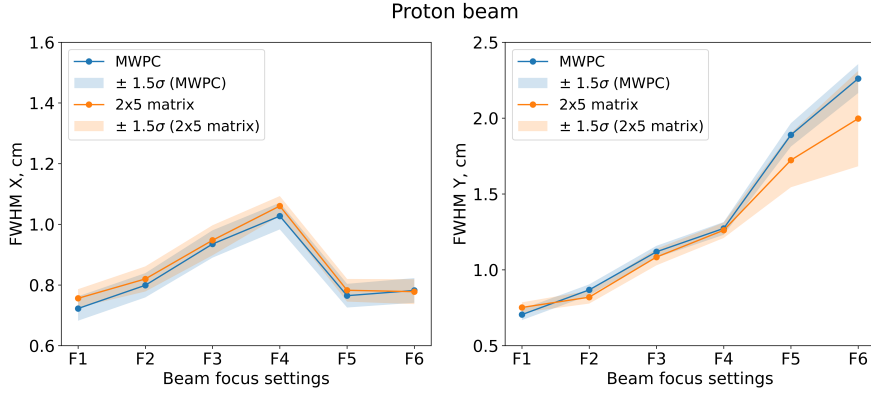


**Figure 7.** Measured mean of FWHM  $x$  (left) and FWHM  $y$  (right) of a proton beam with the HitPix  $2 \times 5$  matrix and the MWPC at different focus settings. Nominal beam parameters: intensity =  $2.0 \times 10^8 \text{ s}^{-1}$ ; energy = 221.06 MeV/u.

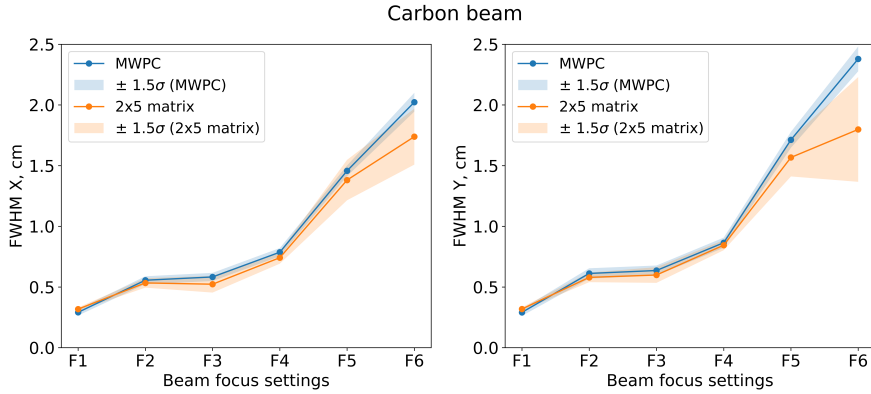


**Figure 8.** Measured mean of FWHM  $x$  (left) and FWHM  $y$  (right) of a carbon ion beam with the HitPix  $2 \times 5$  matrix and the MWPC at different focus settings. Nominal beam parameters: intensity =  $5.0 \times 10^6 \text{ s}^{-1}$ ; energy = 430.1 MeV/u.

## 5 Conclusion

In this article studies with HitPix, a family of monolithic pixelated silicon sensors based on HV-CMOS technology for the beam monitoring at HIT, are presented. The studies were focused on the characterization and resolving issues of the HitPix2 sensor in preparation of the new HitPix3 sensor design which will be used for a  $5 \times 5$  beam monitor demonstrator.

Measurements with a proton microbeam established that the known detection efficiency drop of HitPix2 at high particle rates was caused by a baseline drop of the first stage amplifier when ions hit the pixel region  $200 \times 100 \mu\text{m}^2$  size, which partially covers the sensor diode and transition area between the diode and the in-pixel electronics. The HitPix3 should be produced with the ISO pixel topology and the HitPix1 amplifier design since the measurements also revealed the high tolerance of ISO HitPix1 sensor to this negative effect.

The radiation hardness studies confirm the necessity of an air-cooling system for the future beam monitor demonstrator to compensate the well-known effects of increasing sensor leakage current and noise caused by radiation damage. Sensors with different resistivities were uniformly irradiated with

23 MeV protons and fluence  $\sim 1 \times 10^{15} \text{ cm}^{-2}$  and used in measurement with steady carbon beam at different sensor temperatures. According to these measurements, HitPix3 should be implemented on a  $300 \text{ Ohm} \times \text{cm}$  substrate, which has the best performance after irradiation. The new design should include an individual in-pixel comparator threshold tuning, since a single threshold value for all pixels led to a fraction of  $\sim 25\%$  pixels being masked due to their higher noise after irradiation.

A matrix prototype with two rows of five HitPix2 sensors each was assembled and tested. Sensors in one row were connected in daisy chain mode. Comparative measurements of steady proton and carbon beam shapes at different focus settings with the MWPC detector and the HitPix matrix confirmed that the matrix based on HitPix2 matches the HIT requirements in beam shape estimation. The rows of the future  $5 \times 5$  beam monitor demonstrator based on HitPix3 will be assembled in daisy chain mode.

All new features mentioned above were successfully implemented in HitPix3 design. The HitPix3 sensor has been submitted for production.

## Acknowledgments

The authors would like to thank Rudolf Schimassek for his contribution to the DAQ system and GECCO board, Horacio Mateos for the assembly and bonding, Bernd Berger for performing the irradiations at the cyclotron, Stephan Brons, Pietro Marchesi and Lorena Hahn for their help during the beam test at HIT, Ekaterina Trifonova and Robert Lahmann for their contribution and help during the microbeam tests, Zdravko Siketić and the team of the Laboratory for ion beam interactions RBI for providing invaluable help and assistance at the microbeam setup.

This research was supported by the Heidelberg Karlsruhe Strategic Partnership (HEiKA), the KIT Center Elementary Particle and Astroparticle Physics (KCETA), Helmholtz Program Matter and Technology, German Federal Ministry of Education and Research within the programm “Bildgeführte Diagnostik und Therapie — Neue Wege in der Intervention” under Grant 13GW0436A (ARTEMIS). The ion microbeam measurements were done within the frame and financial support of the RADIATE Project (23003103-ST).

## References

- [1] O. Jäkel, G. Kraft and C.P. Karger, *The history of ion beam therapy in Germany*, *Z. Med. Phys.* **32** (2022) 6.
- [2] A. Hoffmann et al., *MR-guided proton therapy: a review and a preview*, *Radiat. Oncol.* **15** (2020) 129.
- [3] A. Dierlamm et al., *A Beam Monitor for Ion Beam Therapy Based on HV-CMOS Pixel Detectors*, *Instruments* **7** (2023) 9 [[arXiv:2211.06113](https://arxiv.org/abs/2211.06113)].
- [4] I. Perić et al., *High-Voltage CMOS Active Pixel Sensor*, *IEEE J. Solid State Circuits* **56** (2021) 2488.
- [5] I. Perić, *A novel monolithic pixelated particle detector implemented in high-voltage CMOS technology*, *Nucl. Instrum. Meth. A* **582** (2007) 876.
- [6] M. Jakšić et al., *In-air ion beam analysis with high spatial resolution proton microbeam*, *Nucl. Instrum. Meth. B* **371** (2016) 185 [[arXiv:1903.04487](https://arxiv.org/abs/1903.04487)].
- [7] A. Weber, F. Ehrler, R. Schimassek and I. Perić, *High-Voltage CMOS Active Pixel Sensor Chip With Counting Electronics for Beam Monitoring*, *IEEE Trans. Nucl. Sci.* **69** (2022) 1288.

- [8] A. Weber, *Development of Integrated Circuits and Smart Sensors for Particle Detection in Physics Experiments and Particle Therapy*, Ph.D. Thesis, University of Heidelberg, Heidelberg, Germany (2021) [[DOI:10.11588/heidok.00030650](https://doi.org/10.11588/heidok.00030650)].
- [9] H. Spieler, *Semiconductor Detector Systems*, Oxford University Press (2005) [[DOI:10.1093/acprof:oso/9780198527848.001.0001](https://doi.org/10.1093/acprof:oso/9780198527848.001.0001)].
- [10] C. Schoemers et al., *The intensity feedback system at Heidelberg Ion-Beam Therapy Centre*, *Nucl. Instrum. Meth. A* **795** (2015) 92.

2024 JINST 19 C03043